Journal of Alloys and Compounds 539 (2012) 129–136

Contents lists available at SciVerse ScienceDirect

Journal of Alloys and Compounds

journal homepage: www.elsevier.com/locate/jalcom

Thermoelectric power factor enhancement of AZO/In-AZO quantum well multilayer structures as compared to bulk films

Sean Teehan *, Harry Efstathiadis, Pradeep Haldar

College of Nanoscale Science and Engineering, University at Albany, State University of New York, 257 Fuller Road, Albany, NY 12203, USA

ARTICLE INFO

Article history:
Received 10 January 2012
Received in revised form 28 March 2012
Accepted 6 April 2012
Available online 9 May 2012

Keywords:
Thermoelectrics
Al-doped ZnO
Interface roughness
Quantum well multilayers

ABSTRACT

This study investigates and demonstrates the enhancement in thermoelectric power factor for n-type AlZnO/InAlZnO multilayer quantum wells as compared to their counterpart bulk films. A 10–20% improvement is observed for operating temperatures <700 °C. Fabricated structures are composed of 50 periods, with targeted individual layer thicknesses of 10 nm. The best performing multilayer shows an electrical resistivity and Seebeck coefficient of 1000 μV/K and at 700 °C. In addition, a theoretical relationship is derived between the thermoelectric performance and correlating microstructure that demonstrates the deterioration of electronic transport properties at increased interface roughness levels. To determine the microstructure and interface roughness of the films, X-ray and spectroscopy techniques were used. The proposed model is based on how quantum well-width fluctuations caused by increased interface roughness leads to the localization of carriers and thus a decrease in electrical conductivity.

© 2012 Elsevier B.V. All rights reserved.

1. Introduction

Today, most of the energy resources used in industrial processes are discharged as waste heat into the environment. Such exhaust heat accounts for approximately 60% unused energy. Hence, thermoelectric (TE) energy conversion, which converts waste heat into electricity, has received much attention. The conversion efficiency of a thermoelectric material is determined by the dimensionless figure of merit, $ZT = \alpha^2 T/\rho\kappa$, where T is the absolute temperature, α is the Seebeck coefficient, and ρ and κ are the electrical resistivity and thermal conductivity, respectively. However, the three physical parameters comprising Z are all functions of the carrier concentration, n. Taking α and ρ to be directly related, and ρ and κ varying inversely to one another (the Wiedemann–Franz law), the improvement in ZT is not an easy task. Currently available thermoelectric materials have a ZT of less than ~1 and the device efficiency of producing electric power rarely exceeds 5%. This performance has limited TE generators to niche applications where requirements for remote operation, reliability, no moving parts, and silent operation have outweighed the more negative aspects of high cost and low conversion efficiency. It is estimated that with a $ZT > 2$ and a temperature difference of 200 K, a 10% heat-to-electric conversion efficiency can be obtained which would make this technology more feasible for mainstream applications [1,2].

Some thermoelectric materials being researched today are nanocomposite alloys of conventionally known TE materials such as Bi_2Te_3, PbTe and SiGe doped with additional impurities. An example is La-doped PbTe–Ag_2Te nanocomposite which uses the Ag_2Te precipitates to enhance phonon scattering while La-doping allows for carrier concentration control and results in ZT values of >1.5 at 775 K [3]. A secondary set of materials include skutterudites, which use a mechanism of impurity void filing, which have resulted in n-type ZT values of up to 1.7 for $CoSb_3$ compounds [4]. However, these materials are commonly toxic, low in abundance as natural resources, and thus not environmentally benign. Based on these disadvantages, metal oxides have emerged as an alternate potential candidate for high temperature thermoelectric applications. In addition to their temperature stability and resistance to oxidation, they can also be deposited via a variety of feasible techniques that are easily scalable. However, the main concern is that conventional metal oxide films have exhibited relatively low levels of ZT (~0.34 at 1000 °C) due to poor carrier mobility from their ionic structures [5].

The well known and highly investigated p-type superconductor, $NaCo_2O_4$, was the first metal oxide observed to show promising thermoelectric properties. Upon further research, the layered structure of $Ca_3Co_4O_9$ has emerged as the leading material candidate with a ZT of 1.2–2.7 at 600 °C [6,7]. This is attributed to the alternate stacking of hexagonal Ca_2CoO_3 layers and rectangular rock salt layers, which results in increased phonon scattering and significantly reduced κ. A second approach is to reduce the ionicity of the metal–oxygen bonds in order to increase the carrier mobility, an example being ZnO-based thermoelectrics. Currently, the most widely studied n-type material is Al-doped ZnO (AZO), which has obtained a ZT value of 0.1 at 1200 °C [8]. More recently, by

* Corresponding author. Tel.: +1 845 661 8905; fax: +1 518 292 7379.
E-mail address: steehan@uamail.albany.edu (S. Teehan).

0925-8388/$ - see front matter © 2012 Elsevier B.V. All rights reserved.
http://dx.doi.org/10.1016/j.jallcom.2012.04.029

means of co-doping with additional low level impurities (Ga or In), an enhancement of *ZT* was found. This is either due to an amplification in the phonon scattering at the increased number of interfaces, or the enhancement in the electrical transport properties from raising the density of the states which coincides with the addition of carrier electrons [9,10]. However, *ZT* values for n-type films remain inferior for practical applications.

The use of lower dimensionality materials has been theoretically proven to be an underlying mechanism in improving the thermoelectric properties of materials, predicting *ZT* values >3 [11]. Some low dimensional structures include quantum wells (QWs), superlattices, quantum wires, and quantum dots. Within these low-dimensional regimes where quantum effects are dominant, the energy spectra of electrons and phonons can be controlled by altering the size of the structures which allows for the manipulation of the material properties. In theory this regime gives rise to new materials even though the material is made up of the same atomic structure as its parent bulk material. Multilayer QWs also known as superlattices, consist of more than 50 periods with individual layer thicknesses of <20 nm [12]. The first material acts as the active layer while the second material with a larger band gap acts as a barrier for the charge carriers. The band-gap offset thus creates a well that is periodically repeated throughout the multilayer [13]. Fig. 1, is the structural design of our samples which utilize the in-plane transport of heat and current flow (parallel to the substrate), whereas conventional TE-based superlattices highlight the reduction of thermal conductivity via cross-plane transport flow [14]. From the in-plane transport methodology we benefit from (a) enhanced density of states near E_F, which results in an enhanced Seebeck coefficient and (b) an increase in the energy-dependence of the carrier mobility $d\mu(E) = dE$ which results from increasing the scattering time's energy dependence, by preferentially scattering electrons depending on their energy (quantized energy band levels). In addition, by using the in-plane transport structural geometry we can obtain much greater distances between heat source and sink which allows for a lower heat flux, $q_x = \kappa\Delta T/x$, where ΔT is the temperature differential and x is the distance.

To obtain feasible devices it would be essential to scale-up this technology to large area substrates. For this reason an appropriate deposition technique must be chosen and verified. Molecular beam epitaxy and atomic layer deposition are deposition techniques which provide excellent precision for ultra thin layers thicknesses, but have low throughput due to low growth rates. Out of all the techniques available, RF sputtering provides high quality films at high growth rates, and is relatively easy to scale up to provide feasible large area depositions as needed for alternative energy applications. However, one well known issue coinciding with the high growth rate of RF sputtering is the increased levels of surface roughness. For our device design optimization it is essential to optimize the TE properties of the 10 nm QWs which means we must understand the impact of well-width fluctuations caused by interface roughness (IFR). We have developed a model which correlates the dependence of electrical resistivity to IFR. For the multilayer stacks under investigation the achievable roughness level from deposition becomes extra critical because initial layer roughness will subsequently impact the layer roughness deposited thereafter.

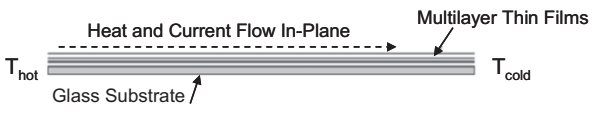

Fig. 1. A representative diagram of our multilayer QW thermoelectric design, using in-plane heat and current transport (Not to scale).

In this work we deposit, characterize, and measure the thermoelectric performances of multilayer QWs consisting of 50 alternating periods of AZO and (In, Al) co-doped ZnO with 2–10 at.% indium. Within this paper we will refer to these samples as InAZO2, InAZO5, InAZO8, and InAZO10 which correspond to 2 at.% In doped $Al_{0.02}ZnO$, 5 at.% In doped $Al_{0.02}ZnO$, 8 at.% In doped $Al_{0.02}ZnO$, and 10 at.% In doped $Al_{0.02}ZnO$ films, respectively. In addition, we will compare thermoelectric performance to previously investigated bulk films of the same materials. Furthermore, we will discuss our newly developed theoretical model relating the electrical resistivity dependence on interface roughness and the subsequent fit to our experimental data obtained via X-ray analysis.

2. Experimental details

Bulk and multilayer films have been deposited using a stainless steel physical vapor deposition reactor equipped with two confocal magnetron sputtering guns. The guns were driven independently by 13.56 MHz rf power supplies. A computer controlled automated system was used to operate the opening and closing of the target shutters in order to control the co-doping process. The targets were commercially sintered 3″ disks of Al_2O_3 (2 wt%)-doped ZnO (99.99% purity, Plasmaterials Inc.) and indium (99.95% purity, Plasmaterials, Inc.). Preceding all depositions, the reactor was evacuated using a combination of a mechanical pump and turbomolecular pump to a base pressure of $<5 \times 10^{-7}$ Torr. In order to vary the Indium in film concentration between 2 and 10 at.%, the In target RF power was increased from 10 to 20 W accordingly [14]. Preliminary baseline experiments were performed on AZO to optimize the deposition in terms of high crystallinity, low resistivity, and low root mean squared (RMS) surface roughness. The process parameters are Ar/O_2 gas ratio of 3, 2 mT operating pressure, 100 W AZO target power, and a 150 °C substrate temperature which is located 40 cm from the target. For comparison purposes all films, both bulk and multilayer films have a total targeted thickness of 1 μm.

The 50 periods of AZO/InAZO multilayer QW films are deposited with a targeted individual layer thickness of 10 nm, because this will result in quantum well effects (<20 nm). Deposition times varied due to the increased growth rate (1.8–2.7 nm/min) for higher indium RF power (10–20 W) [14]. All films were deposited on 100 mΩ-cm n-type (100) Si wafers as blanket films for characterization purposes. These devices were fabricated by forming 1.5×0.5 cm plateaus of multilayers via reactive ion etching. Chemical selectivity to the Si substrate was not an issue and did not result in any substrate pitting. Devices were then inserted into a custom designed clamp which allows for the Cr/Au electrical contact deposition on the short 0.5 cm ends (Fig. 1) without any subsequent deposition on the top/bottom of the sample. This was done on the samples with multilayer structures as well as just on the substrate, in order to allow for the separation of Seebeck coefficient measurements [15]. This will be explained in further detail in the Section 3.2. In addition, the substrates were cleaned using the standard RCA method, and subsequently dried with N_2.

3. Results

3.1. Structural and morphological properties

Samples deposited consisted of 50 periods of 10 nm layers with QWs ranging from 0 to 10 at.% indium, resulting in a total thickness of 1 μm. Phase identification was carried out on a Scintag X-ray diffractometer (XRD) equipped with a Cu Ka1 X-ray source and a horizontal wide-angle four-axis goniometer with stepping motors which allowed for independent or coupled $\theta/2\theta$ axis motion. The multilayer films were initially annealed for 2 h at 900 °C in atmosphere to allow for necessary re-crystallization and then scanned from 20 to 60°. The collected XRD patters were compared to reference patterns from the standard Joint Committee for Power Diffraction Standards powder diffraction file. For comparison purposes, all sample data has been normalized to its maximum peak intensity.

After normalization, the results obtained are identical to the bulk XRD patterns obtained in a previous investigation of (In, Al) co-doped ZnO bulk films [7]. The XRD pattern in Fig. 2, show that 0 and 2 at.% In films have a sole detectable diffraction peak, which is nearly consistent with that of the (002) standard ZnO crystal plane. Using the Debye–Scherrer formula the grain sizes for the 0 and 2 at.% indium films are 32 ± 2 and 38 ± 2 nm, respectively. This

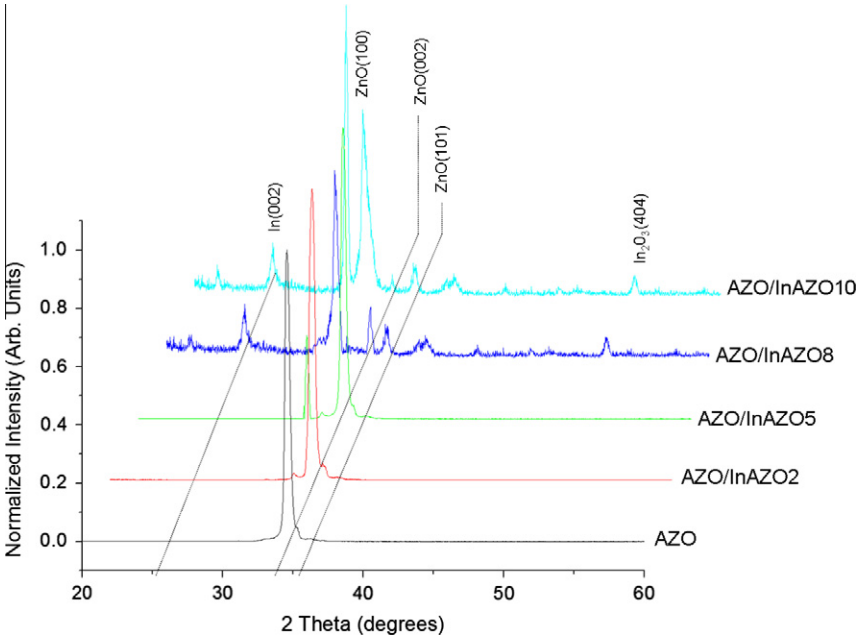

Fig. 2. Bragg diffraction pattern for $Al_{.02}ZnO/In_xAl_{.02}ZnO$ multilayer quantum wells, with $0 \leqslant x \leqslant 0.1$. Note the shift in preferred film orientation from ZnO (002) to ZnO (100) for AZO/InAZO8.

is attributed to the larger atomic radius of indium being incorporated into the ZnO lattice structure. At 5 at.% indium, we observe a (100) ZnO peak that with even further doping becomes the preferred film growth orientation. Also at 8 and 10 at.% indium, In-based peaks materialize which is a sign of elemental agglomeration within the crystal structure.

In thin films analysis's the surface morphology majorly impacts the use of spectroscopy techniques, and for this reason similar we have verified similarity using atomic force microscopy (AFM). A Veeco Dimension 3100 Scanning Probe Microscope at CNSE was used, along with a sharp silicon probe that is ideal for tapping mode at 42 N/m and 320 kHz. The average surface roughness (Ra) was measured from five, 1 μm × 1 μm size scans for each sample and the results were 1.1, 1.3, 1.8, and 3.1 nm for InAZO2, InAZO5, InAZO8, and InAZO10, respectively. For all images taken (Fig. 3), the surfaces appear to be contaminant free and without any significant peaks or valleys. We therefore safely assume that surface variation will not impact our X-ray results. Also apparent is the fact that the AZO/InAZO2 appears to have the smallest grains on the surface which is in agreement with the XRD data obtained from the bulk films. This may be attributed to the lowest lattice mismatch between the barrier and well layers for all the samples.

In order to characterize the microstructure of the QW multilayers in terms of periodicity, layer density, and interface roughness, X-ray reflectivity (XRR) profiles were recorded by a Rigaku Ultima III X-ray diffractometer equipped with parallel beam optics. Parallel beam optics are capable of delivering high-intensity X-ray beams with low divergence. The X-ray mirror provided a high-intensity beam with 0.05° divergence; the divergence slit was set at 0.05 mm to minimize the sample size illumination effects. The acquired XRR profiles were analyzed by the Motofit software package. The sample was modeled as a constant-density multilayer stack of AZO and In-doped AZO. The layers' thickness, density, surface and substrate-film roughness were used as fitting parameters. The software performed the least-squares regression to extract the roughness and density information from the XRR traces.

In Fig. 4, we observe that QW samples with 2–8 at.% indium doping within the well demonstrate an ordered layer structure with excellent periodicity. This is inferred from the well-defined first and second-order reflections. However, the sample with 10 at.% indium doping within the well shows evidence of non-periodicity and non-superlattice behavior. This can be attributed to elemental agglomeration of the indium resulting in a low layer thickness to interface roughness ratio.

In order to verify the XRR analysis, cross-sectional transmission electron microscopy TEM microimages were taken with a JOEL 2010-F FEG TEM operated at 200 kV, shows periodic stacking of the constituent layers of the multilayer film as shown in Fig. 5a. A more high resolution image is seen is Fig. 5b, where we can identify the indium doped wells, which appear as dark layers due to their increase in density. These images are of the AZO/InAZO8 sample and confirm uniform 10 nm layer thicknesses.

3.2. Thermoelectric performance

In order to calculate the thermoelectric power factor (α^2/ρ) of the samples both the electrical resistivity and Seebeck coefficients are needed. The substrate contribution to the electrical resistivity is considered negligible due to the resistivity ratio between substrate and film being >10000:1 [16]. The resistivity was measured both using a 4-point probe at room temperature and a 2-point probe technique from 300 to 975 K. Obtained values were within 2% of each other at RT. By obtaining the total resistance measurement with the 2-probe technique and knowing the sample geometry we can back-calculate the QW structure electrical resistivity. For our devices the measured total resistance includes the QW structure–metal contact resistance and the in-plane QW structure resistance. For this reason, structures of different lengths are used to eliminate the effect of the contact resistance and to obtain the sample resistivity. Obtained results indicate that the contact resistance values are <0.1 mΩ-cm, which accounts for <5% for the lowest resistivity film. Bulk films measurements provided are the results of a previous investigation that used the same measurement techniques [7].

The in-plane Seebeck coefficient measurement is straightforward: building up a temperature difference across the sample and measuring the output voltage, however, in our device the Seebeck coefficient of the substrate (α_{sub}) will contribute to the overall measurement. In order to separate out the sample, a measurement is

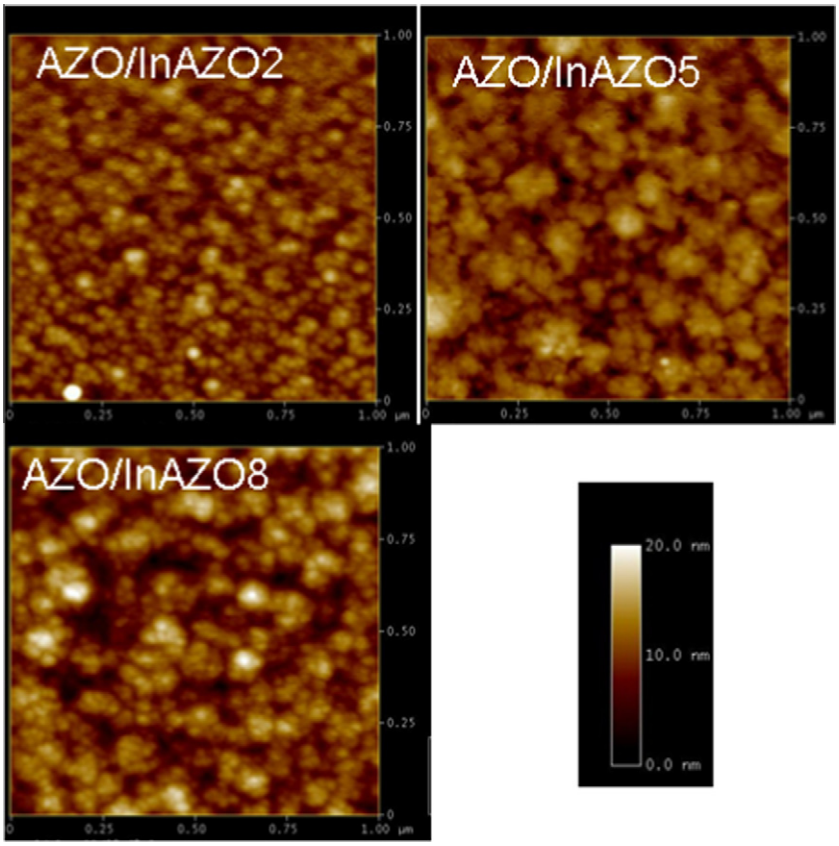

Fig. 3. AFM scans for three multilayer stacks with varying levels of indium doped wells. Results show all films are free of large agglomerations and that grain size increases with increased doping levels.

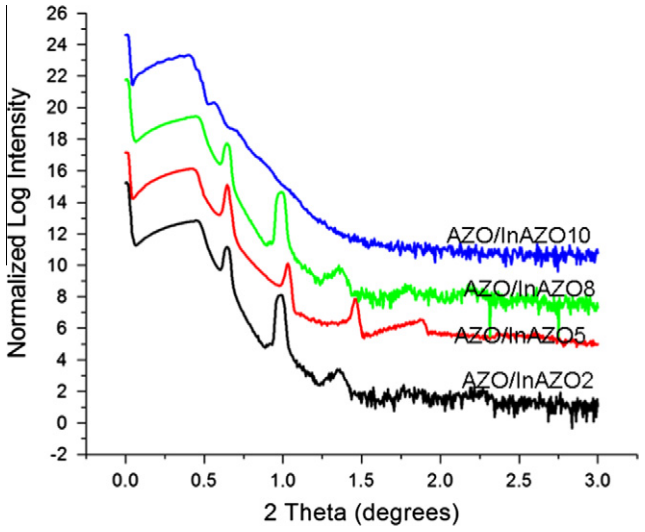

Fig. 4. X-ray reflectivity profiles of 50 periods of AZO/InAZO with various indium doping levels from 2% to 10%. Plots indicate defined reflections for the 2, 5, and 8 at.% indium films which are indicative of good periodicity of the multilayer structures.

performed on both the substrate as well as the combination of substrate and film stack (α_{combo}). We then apply Eq. (1) to our results in order to determine the Seebeck coefficients

$$\alpha_{combo}\Delta T = \alpha_{ML}\Delta T_{ML} + \alpha_{sub}\Delta T_{sub} \quad (1)$$

The Seebeck coefficient setup includes two cylindrical heaters that are bored into copper blocks, each with an independent temperature controller (Omega Inc.). Then by using thermocouples placed at the end of the samples a 50 K temperature gradient was maintained, with the hot side temperature ranging from 325 to 975 K. A voltmeter was soldered onto a nearby position which measured the voltage differential [17].

Fig. 6a–c exhibit the temperature dependent measurements of the in-plane electrical resistivity, Seebeck coefficient, and thermopower, respectively. Fig. 6a and b are experimentally measured, and *c* is a calculation based of the prior. Fig. 6a has been plotted on a log scale in order to show the full range of measured values. We observe that ρ for the QW multilayer structures has been reduced by up to an order of magnitude at specific temperatures (500–750 K) and doping levels (1 and 2 at.% indium). The amount of improvement over the parent bulk films varies for each of the QW structures. For example at 575 K, the electrical resistivity of the QW structures as compared to the In-doped AZO bulk film is improved by 63%, 89%, 91%, and 50% for the 2, 5, 8, and 10 at.% indium doped films, respectively.

Seebeck coefficients were also measured at 50 K intervals between 325 and 975 K and are shown in Fig. 6b. As expected all samples have negative Seebeck coefficients demonstrating n-type behavior. The bulk and multilayer samples both show a linearly decreasing α, with increasing operating temperature. Unlike the ρ measurements we do not see an improvement in α that surpasses the values of the bulk components. The resultant α value is actually an intermediate between that of the two parent films it is composed of. In addition, for all films, we see that with increasing at.% indium concentration there is a trend of decreasing α values. For instance, at 575 K the Seebeck coefficients for InAZO2, InAZO8, and InAZO10 are −143, −202, and −210 μV/K, respectively.

Based on the electrical resistivity and Seebeck coefficient measurements, the thermoelectric power factor was then calculated and plotted against temperature in Fig. 6c. We observe that the

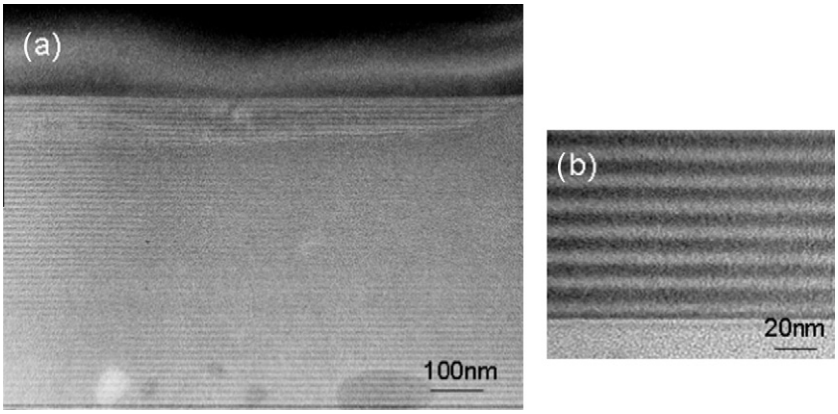

Fig. 5. Cross-sectional TEM images showing (a) full sample QW stack and (b) partial stack w/dark layers indicating indium doped quantum wells.

multilayer structures with 2 and 5 at.% In doped wells show the most promising power factors. Specifically within the temperature range of 550 to 750 K we see an increase in power factor by more than 3*x* as compared to the parent bulk materials. The AZO/InAZO8 multilayer shows an intermediate level of performance as compared to its bulk counterparts, while AZO/InAZP10 shows no improvement.

4. Discussion

Our experimental results indicate that the sample structures have significantly reduced electrical resistivity at low levels of In doping within the QW (2 and 5 at.%) as compared to both the parent bulk films, which is attributed to two main factors. First, a portion of the improvement is material dependent. Thru the addition of a more electrically conductive film ($In_xAl_{0.02}ZnO$) we gain a moderate decrease in the total multilayer structure resistivity. This is proven by the AZO/InAZO10 sample which shows no sign of layer periodicity by XRR, yet measures a resistivity of 50 mΩ-cm at 575 K, which is an intermediate values of the parent films, 105 and 1.7 mΩ-cm for the $In_{0.1}$AZO and AZO, respectively. Secondly, when the resistivity is lower than that of either of the bulk films, this is attributed to enhanced quantum confinement effects within the quantum wells. For example, AZO/InAZO5 measures a resistivity 0.93 mΩ-cm at 625 K, which corresponds to a 55% and 90% improvement over the bulk AZO and InAZO5 films, respectively. From Fig. 6a we also note that similarly to all the bulk films, the resistivity of the multilayer structures also increases with higher operating temperature due to increased scattering. However, at operating temperatures >650 K rate of rise ($\Delta\rho/\Delta T$) is much more significant for the QW structures as compared to bulk films. This in theory can be the result of an increase in multilayer hopping caused by the charge carriers gaining enough thermal energy to cross the band-gap offset of the quantum well [12].

In order to determine the optimum doping level for the QW structure it is important to calculate the thermoelectric power factor due to the inter-dependence between electrical resistivity and Seebeck coefficient. The relationship between % doping in the QW and electrical resistivity in not a simple straight-forward relationship as we have just discussed and Fig. 6a exhibits. However, the Seebeck coefficients, from Fig. 6b show an almost linearly trend of improving α for increasing at.% indium. This is attributed to the increase in polycrystallinity of the ZnO matrix, which results in a reduction in carrier mobility for both phonons and electrons. This has been verified thru XRD analysis (Fig. 2). As a result by taking into account an intermediate level of doping and obtaining high quality films, the TE power factors achieved signify the advantage of utilizing quantum confinement for AZO and (In, Al) co-doped ZnO multilayers at high operating temperatures.

4.1. Interface roughness effect

In order to provide appropriate targets for device fabrication we need to understand the impact of material quality and understand the need for repeatability and fabrication control. From our experimental results we have identified a significant decline in performance for multilayer stacks with high levels of IFR. This agrees with the theory that within a QW any deviation from a perfect interface should impact the electrical conductivity, at that at low temperatures IFR is the limiting mechanism for carrier transport [18]. The following model has been developed based on the fact that roughness at the interface leads to fluctuations in the QW width, which in turn modulates the confinement energies and results in a fluctuating potential for the 2D motion of confined carriers. The fluctuation in band energy is given by the partial derivative of energy *E*, with respect to well width *L*

$$\delta E(r) = \frac{\partial E}{\partial L}\Delta(r) \tag{2}$$

where, *E* is the confinement energy and is given as $\hbar^2\Pi^2/2m_zL^2$, and m_z is the *z*-direction hole effective mass, $\hbar$ is the reduced Planck constant, and $\Delta(r)$ is the interface roughness at a position $r = (x,y)$. The influence of IFR on the mobility of 2D electrons is never precise since the roughness itself is not straight forward to model. This roughness is characterized by a *z*-height Δ and a correlation length Λ, and assumes a Gaussian like form because of the always changing interface structure

$$\langle\Delta(r)\Delta(r')\rangle = \Delta^2 \exp\left(-\frac{|r-r'|^2}{\Lambda^2}\right) \tag{3}$$

Taking into account that the interaction is actually the average over all possible configurations of the IFR, the correlation function is

$$\langle E(r)E(r')\rangle = \left(\frac{\hbar^2\Pi^2\Delta}{m_zL^3}\right)^2 \exp\left(-\frac{|r-r'|^2}{\Lambda^2}\right) \tag{4}$$

where, the variance of the function, with the energy squared, is

$$\left(\frac{\hbar^2\Pi^2\Delta}{m_zL^3}\right)^2. \tag{5}$$

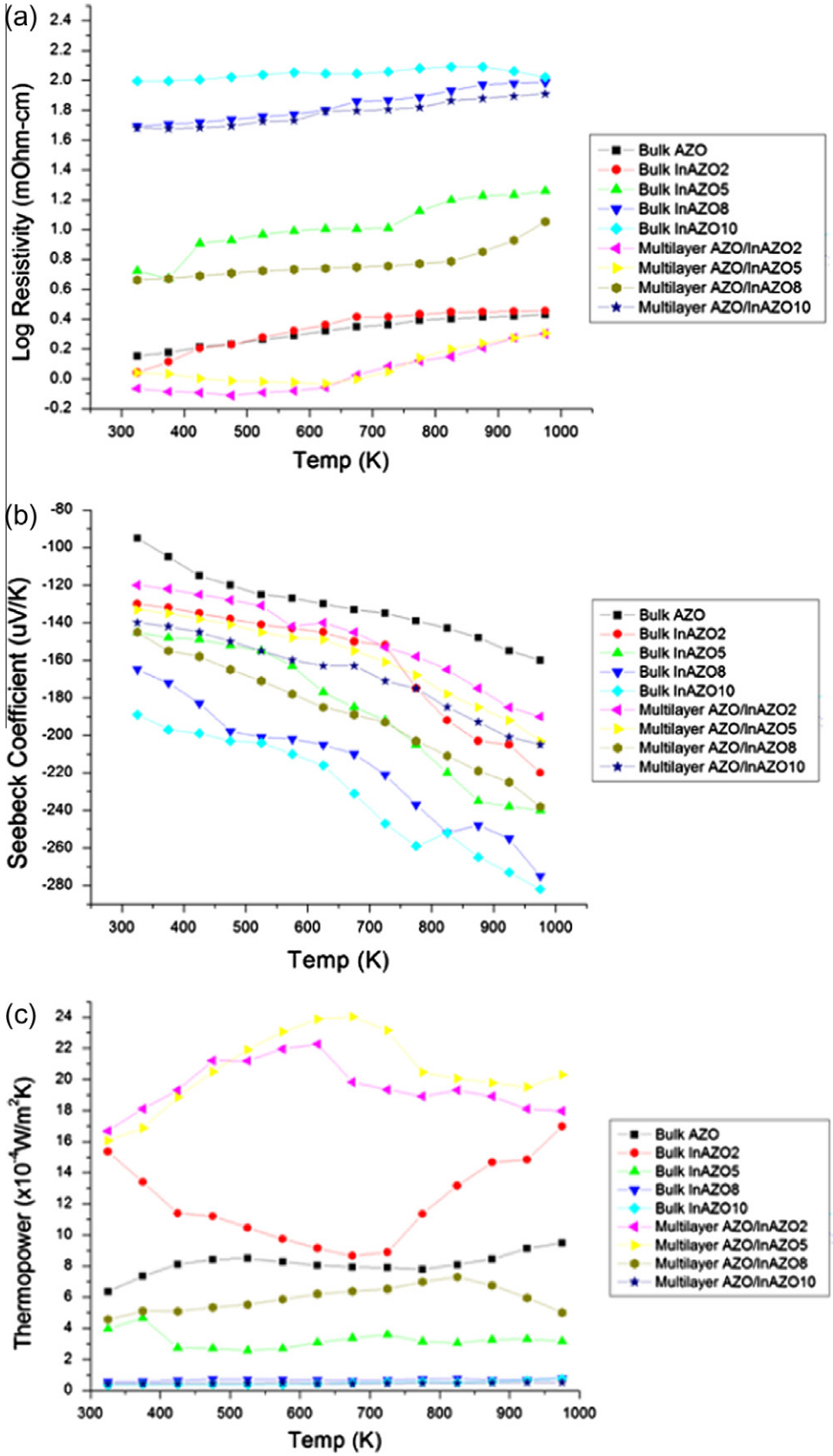

Fig. 6. Plot of electrical resistivity (a), Seebeck coefficient (b), and thermopower (c) vs. temperature for bulk and multilayer films with varying at.% indium. The multilayer films with observed quantum wells show up to a 3*x* improvement in thermopower.

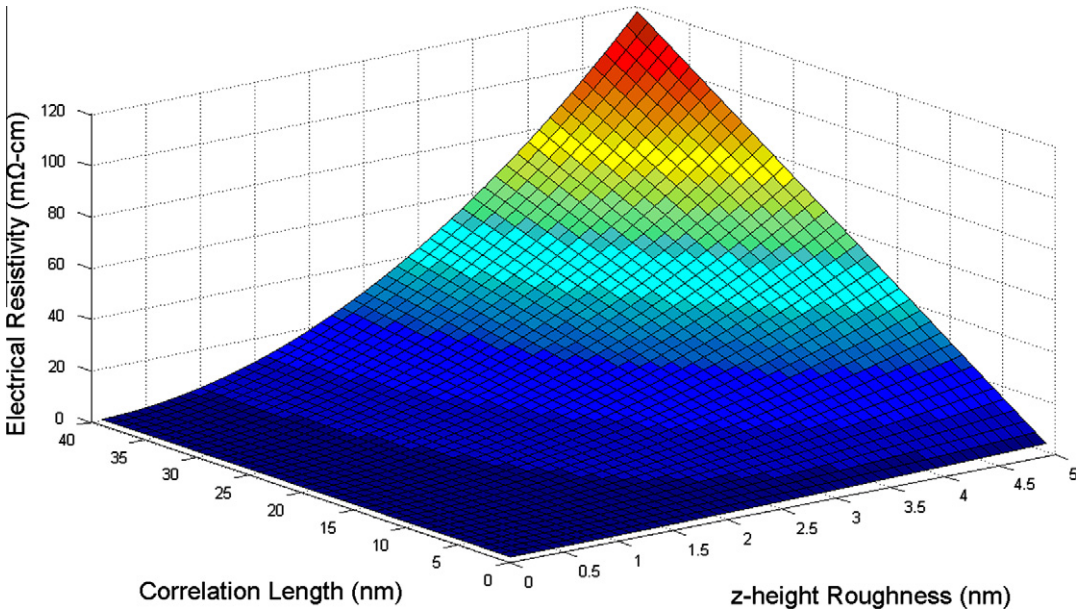

Fig. 7. A 3D plot of resistivity in relation to *z*-height roughness and correlation length for a well-width of 10 nm at room temperature. Resistivity increases exponentially with *z*-height, and linearly with correlation length.

Next, by using a previous derivation we can calculate the electron mobility [19],

$$\mu = \frac{2^{5/2}}{\sqrt[4]{\Pi}} \frac{e}{\hbar} \left(\frac{m_z}{m}\right)^2 \frac{L^6 n_n^{1/2}}{\Delta^2 \Lambda} \tag{6}$$

and include it in our material resistivity calculation, where n is the electron concentration, p is the hole concentration, and μ_n and μ_p are the electron and hole mobility, respectively. For our calculation we consider the impact of holes negligible, due to high n doping.

$$\rho = \frac{1}{q(\mu_n n + \mu_p p)} \tag{7}$$

To model our samples we use roughness RMS values obtained via XRR analysis. The simulated data gives us both well-width and *z*-height roughness (the peak height in the Fourier transform). We estimate the correlation length from the assumed Gaussian form of the IFR. Previously, it has been reported that the IFR can be neglected in quantum wells over 4.5 nm in width [20], but this is only true for a low level of roughness (<1 nm), which would require a deposition technique other than sputtering. More importantly we believe that it is the ratio of interface roughness to quantum well width that is most important.

From the 3D plot in Fig. 7, as well as in Eq. (6), we can see that a change in *z*-height roughness has an exponential affect in determining the sample resistivity, whereas the correlation length impact is linear. It is observed that with Λ values below 2 nm it is possible to achieve resistivity on the order of mΩ-cm for all Δ. Above 2 nm, localized areas with varying potentials will begin to develop due to well-width fluctuations. This difference in potentials leads to carrier localization, and thus higher resistivity.

To complement our theoretical findings, AZO/InAZO5 multilayer samples were analyzed with XRR to obtain a set that are similar in every aspect, yet with varying IFR. The differences in IFR can be attributed to the location as respect to substrate origin during deposition. From best fit XRR simulations we chose four samples with the properties shown in Table 1. In order to estimate the correlation length, we use a Δ measured from XRR, and a calculated Λ, based on a previously determined Gaussian relationship [12]. Both the measured and calculated values are shown here in Table 2. The percent error between the measured and calculated values is within 10%, except for sample 1019_c which has a substantially higher level of roughness. From this we can conclude that our model works for samples levels of roughness for 1.5 nm or lower, roughly 15% of well-width. It is our theory that with increasing IFR the charge carrier localization builds up enough so that a breakdown of the quantum-well effects occurs, which results in an exponential increase in electrical resistivity, i.e., Sample 1019_c. It is therefore evident that consistent and uniform low levels of roughness within the multilayer QW structure are of high concern when scaling-up of this technology. The roughness values shown here may appear large in comparison to previously reported numbers of 0.1 to 0.4 nm for GaN/AlGaN films [14], however, this is attributed to the fact that these films were grown by sputtering, not epitaxially. In addition, these values represent the average *z*-roughness over the full 50 periods, and not just a single quantum well.

As compared to commercially available n-type PbTe-based materials, which have a thermoelectric power factor between 0.0008 and 0.0012 W/m^2 K over the temperature range of 500–700 K [21], our results indicate improved properties ranging from 0.0018 to 0.0023 over the same temperature range. In order to draw further conclusions on material performance however we must obtain thermal conductivity measurements at high operating temperatures. In a separate study on Si/SiC multilayer QW structures the in-plane thermal conductivity showed no variation from that of the bulk properties for temperatures up to 300 K [22]. Based on this assumption that our thermal conductivity is a combination of the parent bulk material properties we have then predicted a ZT value of

Table 1
An XRR analysis summary of deposited samples. Measured well-widths are within 2% of the target, and all samples have low IFR. The sample with 10% indium doping represents non-significant data due to the lack of layer periodicity induced from a high level of film roughness.

Sample	Periods	Width (nm)	IFR (nm)
AZO/InAZO2	50	9.8	1.0
AZO/InAZO5	50	10.2	1.3
AZO/InAZO8	50	10.1	1.4
AZO/InAZO10	50	24	23

Table 2
Summary of IFR values for four 50 period AZO/$In_{0.05}$AZO multilayer structures and their respective measured and calculated electrical resistivity at 325 K.

Sample ID	Details	W (nm)	Δ (nm)	Λ (nm)	Δ/w	$\rho_{calc.}$ (mΩ-cm)	$\rho_{meas.}$ (mΩ-cm)	% Error
1009_a	50 periods/AZO/$In_{0.05}$AZO	10.	1.4	7.8	0.14	10.4	9.5	8.6
1009_b	50 periods/AZO/$In_{0.05}$AZO	9.9	2.1	19.5	0.21	44.4	42.3	4.7
1019_c	50 periods/AZO/$In_{0.05}$AZO	10.1	4.1	33.2	0.41	343	413	20.4
1025_b	50 periods/AZO/$In_{0.05}$AZO	10.2	1.3	8.9	0.13	10.2	9.4	7.8

1.3–1.5 for the AZO/$In_{0.05}$AZO sample at 600 K. Other studies however have shown that both the multilayer interfaces and poly-crystalline grain boundaries will act as scattering mechanisms for phonons [23], which makes it possible that the QW structure will reduce the thermal conductivity, which would ultimately result in even a larger *ZT*.

5. Conclusions

In conclusion, high quality multilayer structures of Al-doped ZnO and (In, Al) co-doped ZnO layers have been deposited using RF sputtering. The fabricated multilayer quantum well structures deposited show a reduction in electrical resistivity by an order of magnitude at 2% and 5% indium well doping as compared to the bulk films. This combined with material dependent Seebeck coefficient enhancements results in a 3*x* increase in thermoelectric power factor and an estimated *ZT* of 1.3–1.5 for the AZO/$In_{0.05}$AZO multilayer quantum well sample at 600 K. In addition, the local flatness of the multilayer structure has proven to be critical for achieving optimum thermoelectric performance. Multilayer samples deposited resulted in a wide range of IFR ranging from 10% to 40% of the well-width. From experimental and theoretical calculations it is desired to have an IFR to well-width ratio <0.1 in order to have optimized thermoelectric transport within the multilayer structure.

References

[1] Science Based Approach to Development of Thermoelectric Materials for Transportation Applications: A Research Roadmap, DOE FCVT, 2007.
[2] T. Hendricks, W. Choate, Engineering Scoping Study of Thermoelectric Generator Systems for Industrial Waste Heat Recovery, Department of Energy Industrial Technologies Program, 2006.
[3] Y. Pei, J. Lensch-Falk, J. Toberer, D. Medlin, G, Snyder, High thermoelectric performance in PbTe due to large nanoscale Ag2Te precipitates and La Doping. Journal of Advanced Functional Materials, 2011.
[4] X. Shi, S. Bai, L. Xi, J. Yang, W. Zhang, L. Chen, J. Yang, Realization of high thermoelectric performance in n-type partially filled skudderudites. Journal of Materials Research, 2011.
[5] P. Pichanusakorn, P. Bandaru, Nanostructured thermoelectrics, Materials Science and Engineering R67 (2010) 19.
[6] R. Funahashi, I. Matsubara, H. Ikuta, T. Takeuchi, U. Mizutani, S. Sodeoka, Bi-substitution effects on crystal structure and thermoelectric properties of $Ca_3Co_4O_9$ single crystals, Japan Journal of Applied Physics 45 (2000) 4131.
[7] R. Funahashi, I. Matsubara, H. Ikuta, T. Takeuchi, U. Mizutani, S. Sodeoka, An oxide single crystal with high thermoelectric performance in air. Japan Journal of Applied Physics, 2000.
[8] H. Yamaguchi, Y. Chonan, M. Oda, T. Komiyama, T. Aoyama, S. Sugiyama, Thermoelectric properties of ZnO ceramics co-doped with Al and transition metals, Journal of Electronic Materials 40 (2011) 723.
[9] M. Ohtaki, K. Araki, K. Yamamoto, High thermoelectric performance of dually doped ZnO ceramics, Journal of Electronic Materials 38 (2009) 1234.
[10] S. Teehan, H. Efstathiadis, P. Haldar, Enhanced power factor of Indium co-doped ZnO:Al thin films deposited by RF sputtering for high temperature thermoelectrics, Journal of Alloys and Compounds 509 (2011) 1094.
[11] L.D. Hicks, M.S. Dresselhaus, Effect of quantum-well structures on the thermoelectric figure of merit, Physics Review B 47 (1993) 12727.
[12] R. Venkatasubramanian, Lattice thermal conductivity reduction and phonon localization like behavior in superlattice structures, Physical Review B 61 (2000) 3091.
[13] G.H. Dohler, Semiconductor superlattices – a new material for research and applications, Physica Scripta 24 (1981) 430.
[14] C. LaBounty, A. Shakouri, J. Bowers, Design and characterization of thin film microcoolers, Journal of Applied Physics 89 (2001) 4059.
[15] S. Teehan, H. Efstathiadis, P. Haldar, Thermoelectric dependence of ZnO:Al/ZnO(Al, In) quantum well multilayer structures on band-gap offsets at high operating temperatures. Submitted to ICT 2011 Conference Proceedings, 2011.
[16] A.V. Wagner, R.J. Foreman, J.C. Farmer, T.C. Barbee Jr., Sputter deposition of semiconductor superlattices for thermoelectric applications. Materials Research Society, 1996.
[17] N.B. Elsner, S. Ghamaty, Thermoelectric performance of Si.8Ge.2/Si heterostructures synthesized by MBE and sputtering. International Conference of Thermoelectrics, 1996.
[18] S. Gokden, R. Baran, B. Balkan, S. Mazzucato, The effect of electrons and phonons scattering from interface roughness and well-width fluctuations on low field mobility of 2D electron gas in GaN/AlGaN heterostructure, Physica E 23 (2004) 114.
[19] J.M. Li, A model for scattering due to interface roughness in finite quantum wells, Semiconductor Science and Technology 20 (2005) 1207.
[20] J.M. Hartmann, P. Holliger, F. Laugier, G. Rolland, A. Suhm, T. Ernst, T. Billon, Growth of SiGe/Si superlattices on silicon-on-insulator substrates for multi-bridge channel field effect transistors, Journal of Crystal Growth 283 (2005) 57.
[21] G. Ren, X. Jia, P. Zhu, C. Zang, H. Ma, X. Wang, In-situ measurement on electrical character of PbTe at high pressure and high temperature, Chinese Physics Letters 22 (2005) 236.
[22] M. Mazumder, T. Borca-Tasciuc, S. Teehan, E. Stinzianni, H. Efstathiadis, S. Solovyov, Temperature dependent thermal conductivity of Si/SiC amorphous multilayer films, Journal of Applied Physics 96 (2011) 093103.
[23] G. Chen, Phonon heat conduction in superlattices and nanostructures, International Journal of Thermal Sciences 39 (2000) 471.